# Biopolymers impact on hygrothermal properties of rammed earth: from material to building scale

Alessia Emanuela Losini, Anne-Cecile Grillet, Linh Vo, Giovanni Dotelli, Monika Woloszyn

# Biopolymers impact on hygrothermal properties of rammed earth: from material to building scale

**Alessia Emanuela Losini [1*], Anne-Cecile Grillet [1], Linh Vo [1], Giovanni Dotelli [2], Monika Woloszyn [1]**

[1] LOCIE, Solar Academy, CNRS, Université Savoie Mont Blanc, 73000 Chambery, France; anne-cecile.grillet@univ-smb.fr (A.-C.G.); monika.woloszyn@univ-smb.fr (M.W.)

[2] Department of Chemistry, Materials and Chemical Engieering "Giulio Natta", Politecnico di Milano, 20133 Milano, Italy: giovanni.dotelli@polimi.it (G.D.)

*Corresponding author; e-mail: alessia.losini@univ-smb.fr

## 1 Abstract

Three biopolymers were tested as rammed earth (RE) stabilizers, evaluating their impact on the hygrothermal behavior from material to building scale. Hygrothermal characterization included the determination of sorption isotherm, water vapor permeability, thermal conductivity at different moisture content, and specific heat capacity. The hygrothermal data were used as input for the simulation at whole-building scale considering combined heat and moisture transfer. The results were evaluated by comparing heating demand, thermal comfort during summer, and the contribution of walls for passively controlling indoor humidity. The results show that hygric properties were only slightly affected by the use of stabilizers, while the thermal conductivity was 33% higher for RE stabilized with lignin, consequently increasing the heating demand at whole-building scale. All RE walls were effective in reducing temperature oscillations in summer. In the particular case of a canicular event, the indoor temperature was reduced by up to 10° compared with the outdoor value. The indoor humidity also benefited from the passive regulation by RE walls, regardless of whether a stablizer was used.

**Keywords:** rammed earth (RE); biopolymers; hygrothermal properties; heat and moisture transfer simulation; building energy performances; HAMT EnergyPlus;

**Abbreviations:** RE (rammed earth), MIX (unstabilized RE specimens), LIG (MIX + lignin sulfonate), TAN (MIX + tannins), WOOL (MIX + sheep wool fibers), EP (EnergyPlus)

**Highlights:**

- Stabilization of RE with lignin sulfonate increases thermal conductivity by up to 30%.
- RE can reduce indoor temperature by up to 10° during canicular events.
- The use of paint on RE walls decreases their contribution to controlling indoor humidity.
- Uninsulated RE walls represent approximately 50% of the total sensible heat losses.

# 2 Introduction

## 2.1 Context and background

The buildings sector accounted for 30% of total global final energy consumption and for 30% of $CO_2$ emissions of total emissions at world scale in 2021, including the indirect emissions from electricity and heat production [1]. Despite the increased activity levels in this sector, the related environmental impacts should be reduced by 45% by 2050 in the scenario for Net Zero Emissions [1]. As an example of national strategy to reach this goal, the new French environmental regulation RE2020 [2] indicates three main objectives for the building and construction sector aimed at reducing anthropic pressure on the environment: a reduction in energy demand and in the carbon footprint of the whole lifecycle of a building while finding new strategies to manage thermal comfort during summer. In this context, the use of earth as a construction material has several advantages, and many researchers aspire to find innovative technologies to exploit its potential. It should be mentioned that about one-third of world population still lives in earthen houses, distributed on all five continents [3,4]. Moreover, earthen sites represent 10% of the World Heritage List of UNESCO [5]. These vernacular techniques of construction are nowadays studied all over the world, producing an exponential rate of publications and research on the subject [5,6].

Raw earth has low embodied energy thanks to local availability, low processing energy during the construction phase, and recyclability [7,8]. Moreover, rammed earth construction offers the potential of re-using non-hazardous waste from excavations, which represents around 7–10 million tons per year in France [7]. In addition to their low environmental impact, some properties of raw earth materials are of interest for the operational phase of a building's life, such as high thermal mass and the capacity to buffer moisture variations. Thanks to their passive regulation of the indoor environment, these buildings are particularly efficient in hot climates, where there is no need for additional insulating material during the mild winter season [9,10]. The literature shows that rammed earth (RE) walls can provide passive regulation of indoor air during summer when adequate sun protection is used in combination with efficient ventilation, in particular during the night [11,12].

RE is one of the popular raw earth construction techniques, widespread in France from the 15$^{th}$ to the 19$^{th}$ centuries, and it represents about 40% of the vernacular buildings in the Isere-Rhône-Alpes region [13] (Figure 1). RE walls are built by compacting layers of soil of about 10-15 cm into formwork using a pneumatic hammer. At the end of the process, the material is able to stand thanks to the combined action of clay, the adequate quantity of water, and the compaction effort applied. A well-graded grain size distribution for the soil is recommended in order to have an adequate percentage of clay, sand and gravel in the mixture [14]. For unstabilized RE, clay is considered the only binder in the mixture and it is classified as raw earth material due to the procedure of drying without a firing process. RE is a porous material, with a high ability to adsorb and desorb water molecules in its porous network, in particular due to the presence of clay particles. Thanks to this ability, earthen materials can simulate similar effects to phase change materials, where the water is free to change phase to maintain the walls in equilibrium with the environmental conditions. At the same time, the strong sensitivity to water represents a risk factor when the moisture content in the material increases over a certain level [15].

*Figure 1: Rammed earth house in the village of St. Chef, Isere, south of France.*

Wider dissemination of raw earthen construction requires improvements in mechanical performance and durability, particularly with regard to leaching. To improve the mechanical strength of this material as well as its resistance to liquid water (rain, capillary rise, etc.), it is common practice to add stabilizers to the soil, notably cement or lime [8,16]. However, this leads to an increase in the environmental impact of the material of more than double with respect to unstabilized RE [8]. At the same time, the stabilization risks reducing the vapor permeability and the moisture buffer capacity [17,18]. In addition, it also involves problems of recyclability, due to the chemical reactions that transform earthen building elements into artificial stone.

In a previous publication [19] the authors presented the first part of this research with the aim of investigating the effect of five biopolymers (citrus pomace, wool sheep fibers, lignin sulfonate, grapeseed flour and tannin) to improve the mechanical performance of raw earth materials while preserving their environmental sustainability. The use of lignin sulfonate, tannins, and wool as bio-stabilizers increased the unconfined compressive strength of the material by approximately 38%, 16%, and 6%, respectively, compared with control samples.

The additives yielding promising results were selected to investigate the impact of stabilization on the hygrothermal properties both at material and at building scale. In the literature, there are some results presented on the modifications of the hygrothermal properties at the material scale when stabilizing the material, but there is a lack of knowledge about the impact at the building scale [17,20,21]. Beckett et al. [22] simulated the thermal behavior of an RE house with an accredited software used in Australia (BERS Pro, v4.3),

without combined heat and moisture transfer. Similar studies are available in the literature, all of which consider only heat transfer through the walls with different commercial tools (TRANSYS, Design Builder) [11,23–25]. The work by Medjelekh et al. [26] is worth mentioning for the combined heat and moisture transfer simulations on unfired earthen bricks wall. Soudani et al. and Gao et al. also presented a study on combined heat and moisture transfer for RE walls. More recently, Tan et al. and Jiang et al. [27,28] investigated the influence of the use of a moisture barrier and non-constant hygrothermal parameters by implementing a heat and moisture transfer model in Comsol to simulate the behavior of an RE wall in northwest Sichuan, China. Finally, Allinson et al. [29] presented the first study with combined heat and moisture transfer via WUFI PLUS at a whole-building scale for RE stabilized with cement; however, there is no information in the literature on earth stabilized with biopolymers.

The present study aims to evaluate the impact of bio-stabilization on the hygrothermal properties of RE from material to building scale. To study the different types of RE stabilized with additives and biopolymers, we adopted an approach of finding experimentally the parameters that describe the physical behavior of the materials to be used as input data in the numerical model that will consider combined heat and moisture transfer.

## 2.2 Hygrothermal behavior of RE materials

The energy performance of RE materials strongly depends on vapor transfers. The description of this phenomena is then explained before presenting the corresponding material properties and their experimental measurements. Combined heat and moisture transfer in hygroscopic material can be described by different models, which enables variations in the properties of the material as a function of moisture and temperature conditions in the material itself. The mathematical model implemented here is based on the theoretical moisture and heat balance equations for the building envelope in one dimension, as described by Künzel, (equations ((1) and (2)) [30,31]. The three terms of equation (1) describe heat storage, heat transfer, and heat generation, respectively, in the building envelope. The three terms of equation (2) refer to the storage of moisture, liquid, and vapor moisture transport, respectively, in the building envelope.

$$\frac{\partial \mathrm{H}}{\partial \mathrm{T}}\frac{\partial \mathrm{T}}{\partial \mathrm{t}} = \frac{\partial}{\partial \mathrm{x}}\left(\lambda \mathrm{w}\frac{\partial \mathrm{T}}{\partial \mathrm{x}}\right) + h_v \frac{\partial}{\partial \mathrm{x}}\left(\frac{\delta \mathrm{a}}{\mu}\frac{\partial(\varphi\, \mathrm{P_{sat}})}{\partial \mathrm{x}}\right) \quad (1)$$

$$\frac{\partial \mathrm{w}}{\partial \varphi}\frac{\partial \varphi}{\partial \mathrm{t}} = \frac{\partial}{\partial \mathrm{x}}\left(\mathrm{Dw}\frac{\partial \mathrm{w}}{\partial \varphi}\frac{\partial \varphi}{\partial \mathrm{x}}\right) + \frac{\partial}{\partial \mathrm{x}}\left(\frac{\delta \mathrm{a}}{\mu}\frac{\partial(\varphi\, \mathrm{P_{sat}})}{\partial \mathrm{x}}\right) \quad (2)$$

where T is the temperature (°C); w is the moisture content in the material (kg/kg); x is the length (m) considering the horizontal direction of the walls; t (s) is the time; $h_v$ is the evaporation enthalpy of water (2 489 000 J/kg); φ is the relative humidity (RH); $P_{sat}$ is the saturation vapor pressure; ∂w/∂φ is the moisture storage capacity, ξ; and $D_w$ ($m^2/s$) is the liquid transport coefficient. The ratio between the vapor permeability of the indoor air volume $\delta_a$ and the water vapor resistance factor μ describes the vapor permeability in the material ($\delta_{wall\_material}$). The resistance factor is defined in formula (3).

$$\mu = \frac{\delta_a}{\delta_{wall\_material}} \quad (3)$$

where $\delta_{wall\_material}$ is the vapor permeability of the wall and $\delta_a$ is the vapor permeability of the air. The thermal conductivity $\lambda_w$, the liquid transport coefficient $D_w$, the water vapor resistance factor μ, and the moisture storage capacity $\partial_w/\partial_\varphi$ are parameters that depend on the moisture level in the material [32].

The heat storage capacity also depends on the moisture content of the material w (kg/kg), with the relationship described in the following equation by Kunzel [30]:

$$\frac{\partial \mathrm{H}}{\partial \mathrm{T}} = (\mathrm{C}_p \rho + C_w \mathrm{w}) \quad (4)$$

where $C_w$ is the specific heat capacity of water (J/(kg·C)); ρ is the density of the material ($kg/m^3$); and $C_p$ is the specific heat capacity of the material (J/(kg·C)).

The complete list of the material properties required for the HAMT model includes porosity ($m^3/m^3$), the moisture sorption isotherm curve ($kg/m^3$), thermal conductivity $\lambda_w$ (W/(m·K)), specific heat capacity (J/(kg·K), vapor diffusion resistance factor $\mu_w$ (–), and liquid transport coefficient $D_w$ ($m^2/s$). In the case of strong hygrothermal coupling, such as for the RE material, these parameters can vary with the adsorption and release of moisture. Consequently, it is important to define the measurement conditions (both

temperature and humidity) precisely in order to describe the behavior of the material at different RH% conditions.

The article is organized into two parts. In the first part (section 3) the different RE materials were tested in the laboratory at the material scale to obtain experimental data to be used as input for whole-scale building simulation, which are described in the second part (section 4) of the article.

# 3 Material properties

## 3.1 Materials and methods

### 3.1.1 Samples preparation

The choice of the methodology for the sample preparation, the soil characterization, and the detailed description of the additives are presented in detail in two previous articles by Losini et al. [19,33]. The unstabilized control samples are abbreviated as MIX, while the samples stabilized with the additives are abbreviated with the first letters of the additives: LIG (MIX + 1wt% of lignin sulfonate), TAN (MIX + 1wt% of tannin), and WOOL (MIX + 0.25wt% of wool). Among the samples, MIX has the higher density (2.19±0.03 g/cm$^3$), LIG and WOOL an intermediate value (2.17±0.03 g/cm$^3$), and TAN the lowest value (2.13±0.01 g/cm$^3$).

Small samples for sorption isotherms were prepared from a single layer of compacted soil, and larger samples for water vapor permeability and thermal conductivity were prepared from a double layer of compacted soil. The compaction process respects the standards of the Modified Proctor Test [34]. A detailed description of the Proctor method is reported in the article by Losini et al. [19].

### 3.1.2 Criteria for reaching equilibrium in hygrothermal tests

The equilibrium criterion used in all the tests of the present article is satisfied when a mass variation lower than 0.01% was reached for 3 consecutive days. Indeed, the criterion from the reference standard ISO 12571:2013 was increased from 0.1% to 0.01%, due to the high density of RE as compared to the common hygroscopic materials with higher porosity [35]. The criterion was modified to 0.05% of mass variation only in the case of 95% RH, due to the difficulty of maintaining stable conditions near 100% RH. Moreover, the

choice of 0.05% is a compromise between the requirement of greater stability in the equilibrium state and maintaining a reasonable time to reach it without the risk of developing mold at a high RH level.

### 3.1.3 Sorption isotherm

The small cubic pieces of samples measured 2.5 cm on each side, with a mass of approximately 40 g each. The dimensions of the specimens were designed to be the minimum acceptable by the standards so as to accelerate the time necessary to reach equilibrium at each RH step.

Before starting the test, all the samples were dried in an oven at 50°C to avoid degrading until equilibrium, using boxes of silica gel placed inside to maintain a dry environment. Once equilibrium was reached, the samples were placed in desiccators to lower their temperature and to measure precisely their dry mass ($m_0$) before starting the experiment. To avoid the risk of fragment loss during weighing, the samples were wrapped in transpiring fabric that enables the transfer of water vapor while preserving the integrity of the samples. Preliminary tests showed that the fabric was nonhygroscopic at the humidity levels used for the test; therefore, the adsorption of water was only attributed to the RE specimen.

Air-locked containers with different saturated salt solutions were used to create different RH% levels. Different salts were used to prepare the saturated solution (i.e., KOH, $CH_3CO_2K$, $MgCl_2$, NaBr, NaC, KCl, and $K_2SO_4$) and the RH produced (9%, 22%, 33%, 58%, 75%, 84%, and 97%) [35,36]. The containers were designed to store the salt solution on the bottom and the samples on a supporting grid. Hygrothermal sensors (precision ±3% RH and ± 0.5°C) were placed inside the containers to monitor the humidity and temperature conditions. A constant temperature of 25°C was maintained by a regulated oven (UNI 110 from Memert Ltd.). A balance with a precision of ±1 mg was used for the test (Ohaus Corporation).

The samples were first placed in containers with the lowest level of RH until reaching equilibrium before continuing at the next RH level. The mass of the samples was recorded every 24 h. The experiment continued for 2 months to test seven RH levels for the sorption isotherm.

The moisture adsorption was calculated in reference to the initial dry conditions with the following formula:

$$u = \frac{m - m_o}{m_o} \quad (5)$$

where $m_0$ is the dry mass and m is the mass measured at equilibrium at different RH levels. At least three samples were used to determine the moisture adsorption/desorption curve and the average of their measurements was used to define the final curve. The standard deviation of the measurement of the three samples was always verified to be lower than 3%.

### 3.1.4 Water vapor permeability

*Sample preparation and conditioning*

The samples for the water vapor permeability test were cut from a double layer of the Proctor. A minimum of four specimens were prepared and tested for each mixture typology and level of RH. A standard deviation lower than 2% in the density of the samples of the same type of mixture was considered sufficient to ensure the reproducibility of the specimens [37].

The samples were left to dry in laboratory environmental conditions (25°C and about 40% RH). The samples were then sealed with aluminum tape on the lateral side so as to maintain a single direction free for the vapor exchange. All the samples were accurately measured to define the surface (about 3.5×3.5 cm) and the thickness (2±0.5 cm) with a micrometer comparator.

The samples were then connected with the open lids of the cup adapted for the test, using silicon latex to seal the contact place and prevent the air leaking. To limit any possible hysteresis effect generated during the drying procedure, all the samples were preconditioned at 8% RH inside airtight containers at 25°C using a saturated KOH salt solution. Once equilibrium was reached, the samples were conditioned at 58% RH and 25°C using a saturated salt solution of NaBr [38].

The samples fixed on the lids were connected to the cups with a saturated salt solution (KOH or $MgCl_2$). An additional layer of aluminum tape was added to prevent air from leaking during the test (Figure

2). The layer of air between the surface of the samples and the saturated salt solution was verified to be constant at 2 cm, as reported in Figure 2.

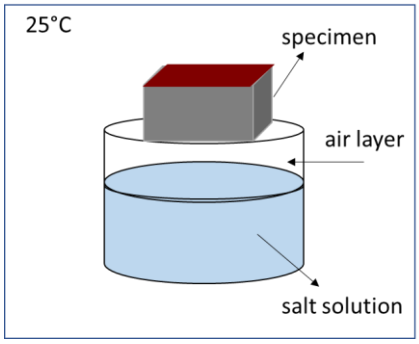


*Figure 2: Diagram of the setup for the vapor permeability test in the RH-Box.*

### *Test procedure*

Water vapor permeability was determined with the wet-cup method based on the EN ISO 12572:2013 standard [39]. The samples prepared with the KOH solution in the cup were placed in the climatic chamber at 33% RH to expose the free surfaces of the specimens at different levels of RH (9–33% RH). The samples prepared with the $MgCl_2$ saturated solution in the cup were placed in the climatic chamber at 75% RH to test the vapor permeability with a different interval of vapor pressure on the two surfaces. The climatic chamber was maintained at a constant temperature of 25°C. Two electronic balances (accuracy ±1 mg) were used to weigh the samples directly inside the chamber. The humidity and temperature levels in the two chambers were recorded and monitored with a hygrothermal sensor provided by Warnet Solutions (precision ±3% RH and ±0.5°C).

The samples were measured four times per day with a minimum of 2 h between two measurements. Due to the difference in the partial vapor pressure outside and inside the cup, water vapor can flow through the specimen. The mass variation between two measurements is calculated with the following equation:

$$\Delta m = \frac{m_1 - m_2}{t_1 - t_2} \quad (6)$$

where $m_1$ is the mass at time $t_1$ and $m_2$ is the mass at time $t_2$ (kg), with $t_1$ and $t_2$ the measurement time (s). The regression line calculated between mass increment and time of measurement, excluding the first part of the nonlinear phase of the test, gives the slope G-line (kg/s). The test continued for about 2 weeks

until reaching a linear variation of mass for a sufficient time to obtain a good correlation in the regression line ($R^2 > 0.999$).

Water vapor permeability δ (kg/(m·s·Pa)) could then be estimated using the following formula:

$$\delta = \frac{d}{\frac{A \cdot \Delta Pv}{G_{line}} - \frac{1}{\beta_{p\,out}} - \frac{d_a}{\delta_a}} \quad (7)$$

where A is the sample area ($m^2$), d (m) is the thickness of the sample, ΔPv (Pa) is the water vapor pressure difference across the specimen, and G (kg/s) is the slope of the line obtained by linear regression on mass and time measurements of the samples. Two correction factors for boundary conditions are present in the formula ($d_a/\delta_a$, $1/\beta_{p\_out}$), where $\delta_a$ (kg/m.s.Pa) is the water vapor permeability of air, $d_a$ is the thickness of the air gap (m), and $\beta_{p\_out}$ is the mass exchange coefficient. The correction is significant for highly permeable materials. The first factor ($d_a/\delta_a$) considers the resistance to the water vapor flow due to the air layer between the sample's surface and the salt solution; the second factor ($1/\beta_{p\_out}$) considers the resistance to the water vapor flow due to the outer boundary layer. In our test facility, $\beta_{p\_out}$ was measured to be equal to $9.8\times10^{-9}$ kg/(Pa.s.$m^2$)), according to Nugyen et al. [40]

### 3.1.5 Thermal conductivity

The thermal conductivity of hygroscopic material depends on its porous structure and the state of pore filling. The three-phase system is composed of soil grains, water, and air at equilibrium with the RH that surrounds the system. The thermal conductivity of liquid water is about 30 times greater than that of air. Consequently, when the pore space is filled by water, thermal conductivity increases. Because of this, thermal conductivity was determined for samples in a dry state and conditioned at 58% and 84% RH.

In the present study, the Hot Disk technology was used, with the advantage of rapid dynamic measurements. The time necessary for one measurement is within the range of 1 min, making it possible to maintain the previously conditioned specimens in equilibrium at a specific temperature and RH.

The thermal measurements were taken with the Hot Disk apparatus (Transient Plane Source method) from ThermConcept (TPS 2500S model). Thermal conductivity and diffusivity were directly measured. The measurement technique is based on the placement of one sensor between two samples, the injection of constant electrical power in the sensor, and the detection of the temperature variation in the samples (Figure

3). A sensor with a double spiral in nickel with Kapton insulation was used for the measurement – model 5501 F1 with a radius of 6.403 mm. The analysis of the temperature rise curves was carried out with the Hot Disk 'Thermal Analyzer' software. The thermal conductivity measurements were carried out according to the manufacturer's recommendations, i.e., (i) the total characteristic time in the range of 0.33 and 1, (ii) the total temperature increase of the sample between 2 and 5°C, and (iii) the standard deviation on the temperature maintained in the range of $10^{-4}$ and $10^{-5}$ K.

The tested samples had the following dimensions: 3×6×4 $cm^3$. The samples were dried in an oven at 50°C for 3 consecutive days until they reached equilibrium in weight. Then the samples were placed in boxes with silica gel near the Hot Disk apparatus to have similar and stable conditions during the test (about 25°C). The other two RH levels were tested, using a saturated salt solution of NaBr and KCl (58% and 84% RH, respectively) to condition the samples.

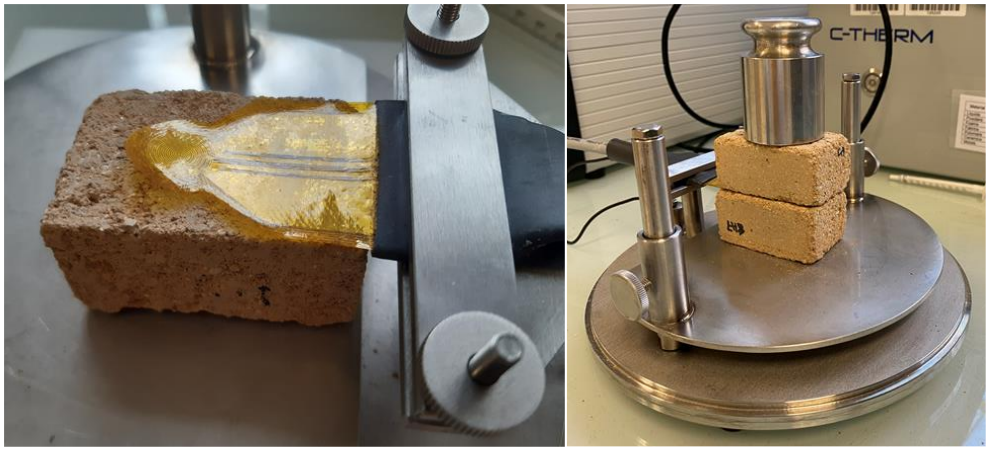


*Figure 3: Hot Disk apparatus sensor and samples positioned during measurements.*

### 3.1.6 Specific heat capacity

In order to measure the heat capacities of materials, we use a DSC-25 from TA Instrument®. The method used is modulated (MDSC, Modulated Differential Scanning Calorimeter) standardized to ASTM E1952 and E2716 with sapphire as the reference standard [41]. The measurements are obtained in a range from 10°C to 50°C with a heating rate of 2 K/min, an oscillation period of 120 s, and an amplitude of 0.64°C.

## 3.2 Results

### 3.2.1 Sorption isotherm

Figure 4 reports the sorption isotherm for the control samples (MIX) and the stabilized mixtures. The shape of the curve suggests a similarity with the type II isotherm described by IUPAC, typical of clayish materials [42]. The use of the additives has a marginal impact on the sorption isotherm, which shows only a very small variation. At a low level of RH% (0–20%), TAN has the highest adsorption, while MIX and WOOL have intermediate values, with LIG having the lowest. In the intermediate levels of humidity (33–85% RH), WOOL has slightly higher adsorption than MIX, and both are reached and surpassed by LIG (Figure 4). TAN shows the highest adsorption at 60% and 80% RH, but it decreases at the higher values of the sorption isotherm. For higher values of RH (84–98%), the values of WOOL, TAN, and MIX are more uniform and LIG presents the highest levels of adsorption, despite showing the lowest adsorption level at low RH%. In general, the samples show a maximum relative change in mass of about 1.8% for 98% RH, which is quite low compared with values from the literature on earthen material with higher clay content that can reach values between 2.5% and 5% of mass variation [43–45]. This behavior may be due to the high content of sand in the mixture (about 80%). Another factor to be taken into account is the drying temperature to determine $m_0$, which was

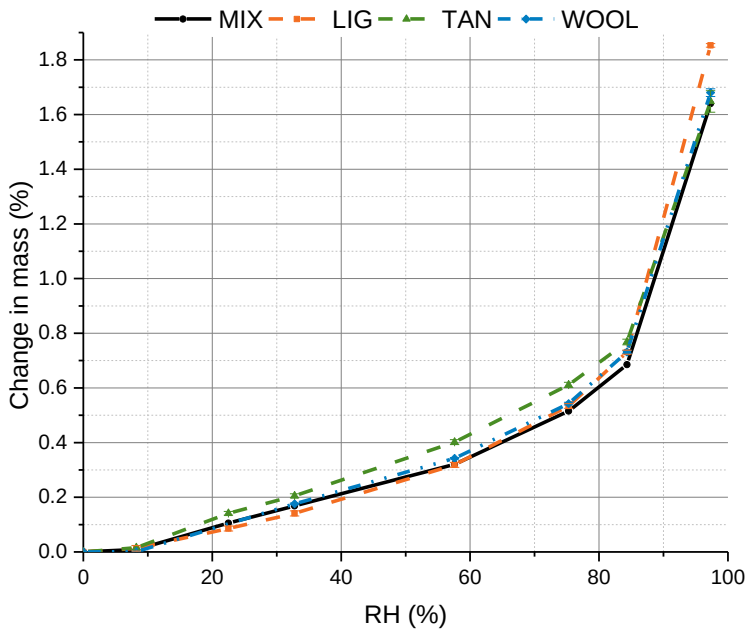


*Figure 4: Sorption isotherm at 25°C.*

chosen to avoid material degradation, in particular, due to the presence of fibers. Different temperatures are proposed in the literature in a range from 55 to 105°C [45–47]. Of course, the use of a different reference for the dry mass can lead to an underestimation of adsorption properties compared to the drying process at 105°C, as illustrated by Fabbri et al. [45].

### 3.2.2 Water vapor permeability

The diffusion of water vapor in a porous material describes the permeance of the material to water vapor transfer under the effect of vapor pressure. It can also be described as a resistance factor (μ), which is the ratio between the water vapor diffusion in the material ($\delta_v$) and the water vapor diffusion in the air ($\delta_a$).

The results are given as an average of a minimum of four samples for both intervals of RH, i.e., 9–33% and 33–75% RH (Figure 5). Considering the variability of the results, this test shows a high standard deviation, which does not enable a clear comparison with the results that have a small variation in values. Some minor tendencies can be seen: The water vapor permeability of LIG is slightly reduced compared to the control samples, while for TAN it is slightly increased. For WOOL specimens the value is slightly decreased for 9–33% RH and equal to that of MIX for 33–75% RH%

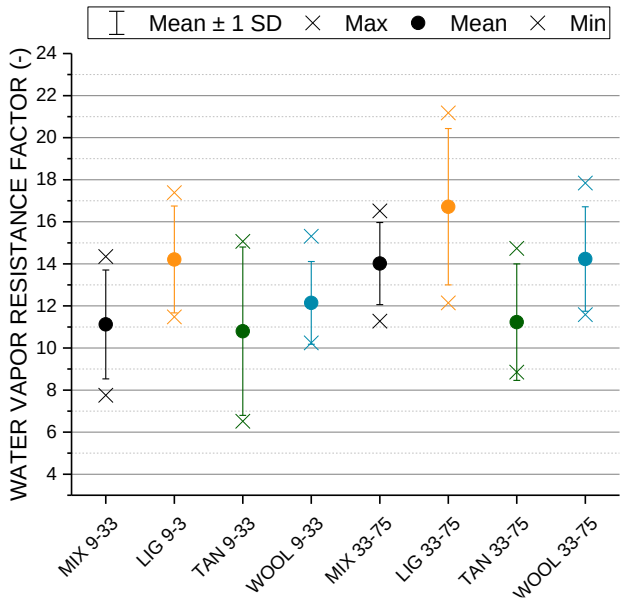


*Figure 5: Water vapor resistance factor measured in two different intervals of RH% (9–33% and 33–75%).*

Generally, for a higher RH, the moisture vapor transfer becomes a mixed-mode liquid–vapor transfer. These phenomena improve the moisture transfer that is higher at higher RH [48]. Conversely, the results of

our study suggest the opposite behavior. However, the increase in the vapor resistance factor is lower than the standard deviation.

Common values of vapor resistance factor for unstabilized RE material in the literature are around 4–10 [47,49], and measurements of stabilized RE with 7% of Portland Concrete showed a value of 14.34 [29], considering the wet-cup method comparison. These values are comparable to fired bricks and cellular concrete but are competitive in relation to standard concrete (B25), which has a value 10 times higher.

### 3.2.3 Thermal conductivity

A couple of samples for each mixture were tested and two couples of samples in the case of WOOL were used to obtain more information about the influence of the non-homogeneous distribution of the wool fibers in the samples. By using four samples (two couples), we can evaluate the variation in thermal conductivity due to different fiber arrangements. The standard deviation between the three measurements is smaller (about 1%) than the average error of the measuring instrument, that is, 5% of the measured values. Thus, the larger value of the measuring instrument (5% of the measured values) was considered.

Thermal conductivity shows a linear evolution with water content, as claimed by many authors for other raw earth materials [13,21,27,47,50]. At the same time, no linear relationship was found between the density and the dry thermal conductivity, in accordance with the findings of Chabriac [47]. The results show a major increase in thermal conductivity for LIG specimens, with values around 1.87 W/(m·K), probably due to the higher density of the samples, while the values for MIX, WOOL, and TAN are around 1.45 W/(m·K). The values of thermal conductivity measured are slightly higher than those in the literature, where they are reported to be between 0.6 and 1.1 W/(m·K )[51]. For the WOOL sample, the value of thermal conductivity decreases compared to the value of the control samples. This is an unexpected phenomenon because the addition of fibers usually decreases the density and thermal conductivity, but similar behavior was found in the literature by Randazzo et al. [52].

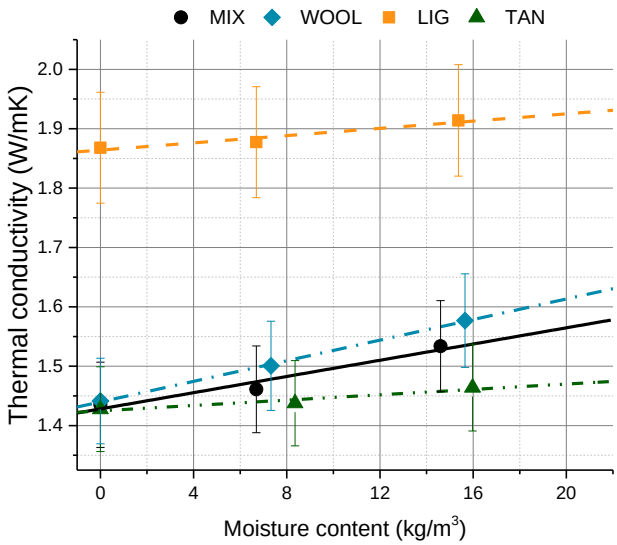


*Figure 6: Thermal conductivity as a function of moisture content.*

Figure 6 displays the thermal conductivity measured in samples conditioned at different RH%. WOOL and MIX show the highest increment of thermal conductivity, estimated by the slope of the linear interpolation, while TAN and LIG show a smaller increase.

### 3.2.4 Specific heat capacity

The results of MDSC (modulated differential scanning calorimetry) on MIX are calculated as an average of the measures in three different samples. The measured value at 25°C was 737 J/(kg·K), in accordance with results from the literature, which reports values between 0.684 and 939 J/(kg·K) for RE materials [47,51].

## 4 Impact at building scale

RE material stabilized with biopolymers has not been exploited in building construction to date, and thus a direct collection of data to obtain experimental measurements at the building scale was not considered a possibility. Moreover, the comparison of different stabilized RE materials involves the use of simulation tools, which enable the comparison of building performance in different case studies and locations, modeling precisely the occupancy scenarios.

The experimental data were used as input for the modeling of coupled heat and moisture transfer using EnergyPlus software. For many years, different tools have been available for simulating coupled heat

and moisture transfer, as presented in the international collaborative project IEA ECBCS Annex 41, Subtask 1 (Whole building heat, air and moisture response). Trnsys, EnergyPlus, and Wufi Plus are some of the software used to evaluate building energy performance, which also enable simulations of coupled heat and moisture transfers. Among the tools, the combined heat and mass transfer model (HAMT) of EnergyPlus was selected for the present work for its widespread use, the possibility to implement detailed scenarios, and the advantage of using free software licenses [31]. EnergyPlus (EP) collects different program modules that work together to simulate energy behavior at a whole-building scale, calculating the energy required to heat and cool a building following operating conditions and external conditions set as input in the simulation. Equations (1) and (2 ) presented in section 2.2 describe the model used in EP for the envelope.

Simulations at the whole-building scale were carried out to evaluate the influence of the different RE formulations on hygrothermal transfers. Five configurations were simulated, using different materials for the vertical walls (MIX, TAN, LIG, WOOL) and in one case the use of painting on MIX walls (P-MIX). Details of the building description, envelope materials, occupancy scenarios, and weather file will be illustrated.

## 4.1 Case study and configuration

### 4.1.1 Building description

#### *Geometry and location*

The test room used in the simulation is based on the well-known BESTEST building, which is used for numerical model validation [53]. It has a total volume of 129.6 $m^3$, the side is 8 m long on the east–west axis and 6 m in north–south direction, for a total floor area of 48 $m^2$, as represented in Figure 7. The wall height is 2.7 m. The building is simulated as one thermal zone.

The windows opening in the building were modified to follow the recommendation for the structural stability of RE construction and to reduce the heating demand using solar gains. In France, the surface area of windows should be at least one-sixth of the living area (*Réglementation thermique* 2012) and the south face of the building is recommended to be heavily glazed, equivalent to 15–20% of the floor area so as to allow for higher solar gains during wintertime. On the other hand, due to the structural requirements for RE construction, the total horizontal length of the opening should not exceed one-third of the total wall length,

with a minimum distance of 0.6–1 m between the opening, 0.75 cm from the corners and 0.45 from above the crown [54]. Moreover, according to Australian standards, the total opening area should not exceed 20% of the total wall area [54]. Finally, four double galzed windows of 1.5 × 1.5 m² each were placed on three sides – two windows on the south wall, one for the east and one for the west walls – resulting in a window-to-wall ratio of 20.8% and 13.9%, respectively, for the façades.

A blind roll of bright aluminum was placed as a screen, located on the exterior side of the window construction. It has a diffuse and visible solar reflectance of 0.6. The blind roll is activated when the indoor temperature exceeds 23°C during summer from June to the end of August.

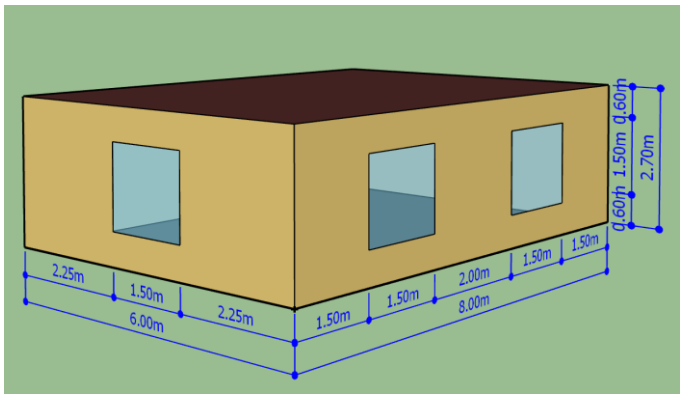


*Figure 7: Test building.*

The location for the building was chosen in Casablanca (Morocco), a city in a region where RE constructions were traditionally built [55]. The annual rainfall precipitation is estimated at around 400 mL and the city is a hot-summer Mediterranean climate zone (Csa) in the Koppen–Geiger Climate Classification [56].

Due to mild winters, no additional insulation is required, enabling a better evaluation of the contribution of RE to thermal comfort and fully exploring its behavior during summer.

### 4.1.2 Walls and construction materials

All four vertical walls of the building are composed of RE materials and their thickness of 50 cm was defined according to international guidelines for RE construction and the current thickness of RE construction in France and Europe [54,57]. Both the roof and the floor are made of a 15-cm-thick concrete slab, with 20 cm of glass fiber insulation on the exterior side of the roof and the interior side for the floor, as presented in Figure 8. The internal layer of the roof is also covered with 1.2 cm of plasterboard ceiling. Table 1 presents the thickness and the principal properties of each material used in the wall assemblies.

Material properties for concrete, plasterboard and glass fiber insulation were taken from the EP library. The properties of the RE materials (MIX, LIG, TAN, and WOOL) required for HAMT simulation were obtained by hygrothermal measurements described in the previous chapter.

The thermal absorbance and solar (visible) absorbance of wall materials taken from the EP library are, respectively, 0.9 and 0.7. The same values were used for RE materials, because they are in line with reports from the literature and they enable easier comparisons between different configurations [10].

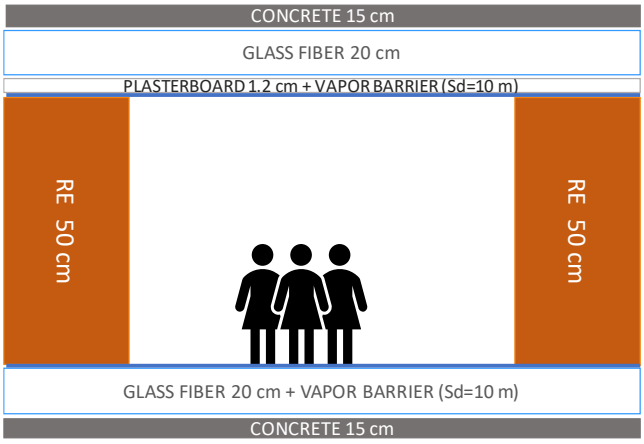


*Figure 8 : Schematic representation of wall assemblies.*

*Table 1: Summary description of material properties used as input for HAMT simulations.*

| Material | | RE MIX | Glass fiber ins. | Plasterboard |
|---|---|---|---|---|
| **Density** | kg/m$^3$ | 2190 | 80 | 250 |
| **Thickness** | cm | 50 | 20 | 1.2 |
| **Thermal conductivity** | W/(m·K) | 1.4-1.8 | 0.04 | 0.2 |
| **Specific heat** | J/(kg·K) | 737 | 850 | 840 |
| **µ1** | - | 11.1 (0.20 RH) | 1.25 (0 RH) | 8.3 (0 RH) |
| **µ2** | - | 14.0 (0.54 RH) | - | - |
| **Sorption isotherm** | kg/m$^3$ | 36.07 (0.97 RH) | 2.27 (0.97 RH) | 23.4 (0.97 RH) |
| **Porosity** | m$^3$/m$^3$ | 0.2-0.23 | 0.95 | 0.65 |

In one configuration, a vapor-tight layer of painting was added on the RE walls of MIX to show and isolate the contribution of RE walls to vapor exchange. This combination was called “painted MIX” (P-MIX). A layer of paint with an equivalent thickness ($S_d$) of approximately 10 m of air was considered on the internal side of the vertical walls.

### 4.1.3 Occupancy scenario

The occupancy scenario is based on a residential building. The summer vacation is not considered and the occupancy is maintained unaltered for all the weeks of the year. An ideal heating system is activated throughout the year at a setpoint of 20°C, and only ventilation systems are used for natural cooling during summer to investigate the efficiency of RE materials in mitigating overheating. No humidification or dehumidification systems are used in order to better assess the effect of the RE walls on regulating the indoor climate.

*Human occupancy and activities*

The residential building hosts three people, who are supposed to work away from home during weekdays. The occupancy schedule reported in Figure 9 is inspired by a literature review performed by Labat et al. [58] and Poirier et al. [59]. The time spent outside the home due to transportation and work amounts to 11 h per day, Monday to Friday from 07:00 to 18:00, while during the weekend the occupants spend 8 h per day away from home mainly during the afternoon (14:00–22:00).

*Sensible and latent load from occupants*

Human presence and human activities are responsible for the emissions of latent and sensible heat, which were defined based on data from the literature [59]. Each person emits 55 g of vapor per hour when awake, and 40 g of vapor per hour during the sleeping period, as shown in Table 2. The sensible heat emissions due to the presence of people are set at 65 W, based on the ASHRAE Handbook indications [60].

Moisture emissions in residential buildings vary depending on activities, as shown, for example, in Table 2 based on Poirier et al. [59]. In our case, the emissions of moisture due to cooking activities and showers have a daily cycle, while laundry and laundry drying are concentrated during the weekend. Preparation of lunch takes place only during the weekend since the occupants are absent during working hours.

Table 2 also presents the daily average moisture production, calculated as grams of moisture per person and as total production in the whole building. The sensible loads are generated by the heat released by human bodies, to which are added the emissions from electrical equipment. The residential building has seven pieces of electrical equipment related to daily life needs: fridge, oven, stovetop, microwave, TV, laptop,

and lamp. Table 3 lists the average power of this equipment and the hours of use per day. The use of light in the dwelling is considered at approximately 5 h per day, with a lighting power equal to 1.4 W/ $m^2$ [61].

Moisture sources are vapor sources and are modeled as "steam production" in EP. It should be noted that the drying process for laundry is different, as it is a liquid source, and latent heat of evaporation must be considered. It is therefore represented in EP as a double source: a positive steam source and a sensible heat source that is set as a negative power of 139.85 W required during the process. In this way, the model considers an amount of sensible heat equal to the negative latent heat necessary to dry the wet clothes and is able to represent a source of liquid water.

*Table 2: Moisture emissions due to different activities in the residential building;* liquid water release. The last two rows report the results of the daily moisture emissions during the weekday and weekend.*

| Activity | Vapor production (g/(h·person)) | Duration /person |
|---|---|---|
| **Sleep** | 40 | 8 h/weekday–9 h/weekend |
| **Awake** | 55 | 5 h/weekday–7 h/weekend |
| **Shower** | 240 | 10 min/day |
| **Breakfast** | 378 | 15 min/day |
| **Lunch** | 1134 | 30 min/day (only weekend) |
| **Dinner** | 1896 | 40 min/week |
| **Laundry** | 252 | 2 h/week |
| **Laundry drying** | 136.8* | 11 h/week |
| | | |
| **Daily moisture production** | Weekday | Weekend |
| Residential (kg/(person·day)) | 3.12 | 6.65 |
| Total residential (kg/day) | 9.33 | 19.96 |

*Table 3: Use of electrical equipment for the residential scenario, based on Stefanoiu et al.* [61].

| Electrical equipment | Average power (W) | Use (h/day) |
|---|---|---|
| **Fridge** | 36 | 24 |
| **Oven** | 1040 | 0.43 |
| **Stovetop** | 778 | 1 |
| **Microwave** | 213 | 0.25 |
| **TV** | 64 | 2 |
| **Laptop/computer** | 90 | 2 |

### *Ventilation*

Ventilation systems, adequate for occupancy scenarios, are designed to guarantee acceptable parameters of indoor air quality. In this study, the ventilation aims to remove a significant part of moisture

production due to occupancy and to ensure a high air change rate during summer nights to cool down the building that collects heat during the hot summer days. Infiltrations are assumed to be included in the ventilation rate.

The residential building hosts different activities during the day, and, consequently, different moisture production rates. The ventilation is adapted not only to the needs of people but also to the need of evacuating the peak moisture due to specific activities such as cooking. The highest level of ventilation suggested by Standard EN15251 guidelines considers 10 L/s/person, which when adapted for three residents is approximately equal to 0.8 volume/h (108$m^3$/h) [62]. The proposed ventilation rate is set to 1 volume/h during cooking (the activity that produces the highest rate of moisture), and 0.7 volume/h during other activities.

A higher ventilation rate is necessary during summer nights to remove the heat stored in the building due to the high temperature reached during the day. From 22:00 to 08:00 the ventilation rate is set at 2 volume/h (277.2 $m^3$/h) from June to August. The complete ventilation schedules are presented in Figure 9.

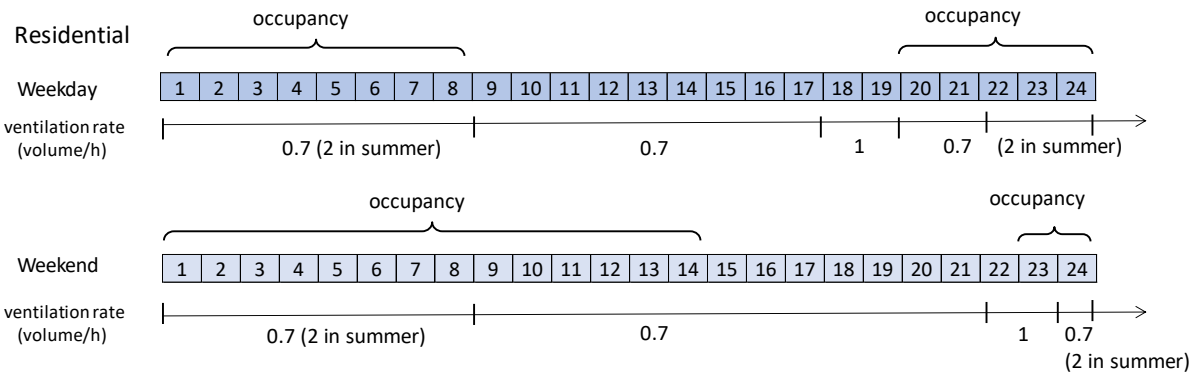


*Figure 9: Occupancy and ventilation rate schedule, for weekdays and weekends.*

### 4.1.4 Initial conditions and run period

The initial moisture content of materials w (kg/kg) must be specified in order to start the simulation. An additional study was carried out to set the initial moisture content at full operative state. Simulations were performed over several years in order to assess the impact of initial conditions. Since the difference between the second and third year was negligible (less than 5%), the run period was set up to 2 years. The

results were analyzed in the second year of simulation only, in order to avoid any possible influence related to the initial conditions.

## 4.2 Results and discussion

The results of the simulation are analyzed from different points of view: the heating demand, the thermal comfort reached with natural ventilation during summer, and the contribution of walls to the passive regulation of indoor air quality. The analysis of the global annual sensible and latent heat balances complements the study and allows for the quantification of the contribution of RE walls to global heat and moisture gains and losses in the different configurations. These global balances are based on averaged yearly values of different energy flows. The balance of sensible heat includes the energy required to increase or decrease the indoor temperature, while the balance of latent heat considers the gain or loss that increases or decreases the moisture content of the indoor air. The sensible and latent contribution from occupancy considers both the heat produced by people and the heat from electrical equipment. The heating system has no impact on humidification or dehumidification and, consequently, it is considered only in the analysis of sensible heat balance.

In the following, the energy fluxes in the balance are described considering as gain (or loss) the increased (or decreased) latent or sensible heat of the indoor air. Of course, instantaneous heat gain in the transient state is generally different from heat loss, since the difference represents the evolution of the system energy (storage). However, by averaging the different fluxes over a significant period (here, for 1 year), energy storage can be neglected.

### 4.2.1 Heating demand and sensible heat

Figure 10 reports the annual heating demand for the reference RE (MIX), the bio-stabilized RE materials (LIG, TAN, and WOOL), and the painted RE (P-MIX). All values are in the range of 36–38 kW/m$^2$, except for RE stabilized with lignin sulfonate (LIG), which reaches 49 kW/m$^2$. LIG shows an increase in heating demand of 32.5% compared with the control samples, while for TAN and WOOL there is a decrease of −3.5% and −3, respectively. The higher heating demand of LIG is probably due to the thermal conductivity that is

higher by about 30% than that of MIX, TAN, and WOOL. P-MIX does not present a significant variation in heating demand compared to MIX.

Considering sensible heat balance, the results for the P-MIX materials TAN and WOOL are very similar to those found for MIX. The heating system and occupancy are the main sources of sensible heat gain for the indoor air volume in all the configurations, representing 30% and 40%, respectively, of the sensible heat gain. The heating system is activated mainly during winter with 20°C setpoint, and therefore the daily occupancy has a major contribution to the heating gain due to its continuity all year long. The remaining significant contributions are made by the floor and the roof, representing 17% and 7%, respectively, of the sensible heat gain. The floor gives off sensible heat to the air due to the solar radiation that is transmitted through the windows and heats the floor surface. The remaining contributions to the heat gain are attributable to the walls and windows.

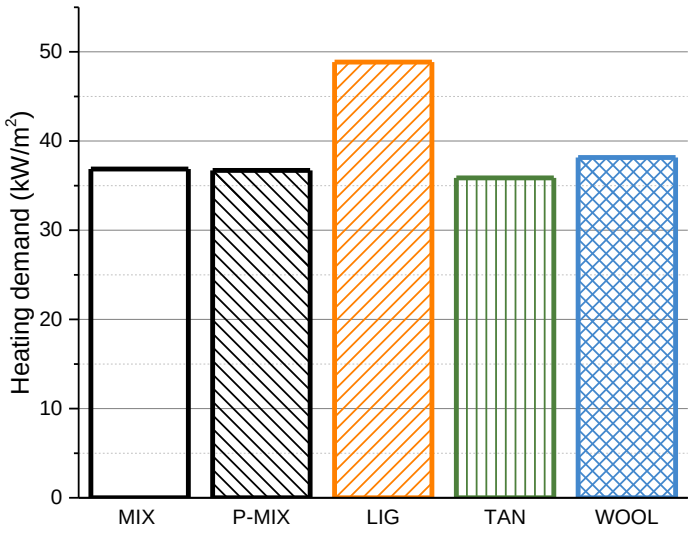


*Figure 10 Annual heating demand.*

Ventilation and transfer through the walls are the main causes of sensible heat loss. The heat loss through RE walls represents approximately 51% of the total sensible heat losses; the remaining contribution is due to the ventilation that is associated with about 32% of heating losses. The remaining contributions to the sensible losses are due to the other walls (including the roof, floor, and windows).

Heat loss due to ventilation mainly occurs during summer nights, in order to efficiently cool down the room without heating the air during the day. The north wall has the highest heat loss (20%) because of

its larger surface and its orientation that limits solar gains, while the other walls have heat losses of about 10% each. The reduced losses are due to position of the sun but also to the reduction of the available wall surface area due to the presence of windows, which are two on the south wall, one in the east and one on the west side.

LIG exhibits a higher sensible loss through the walls, about 55% versus 50% for the other configurations, while the losses due to ventilation are slightly reduced (28%). This is a consequence of higher heating demand for LIG: the lower thermal resistance generates higher heat losses through the walls and, as a result, the relative contribution due to ventilation is slightly reduced.

### 4.2.2 Summer thermal comfort

This section presents the thermal comfort analysis, starting with a comparison of the number of hours where the room temperature is over 28°C (considering the whole year, 24 h/day, including the period of unoccupancy). These data provide the first information on how often the room is in a condition of elevated temperature (Figure 11).

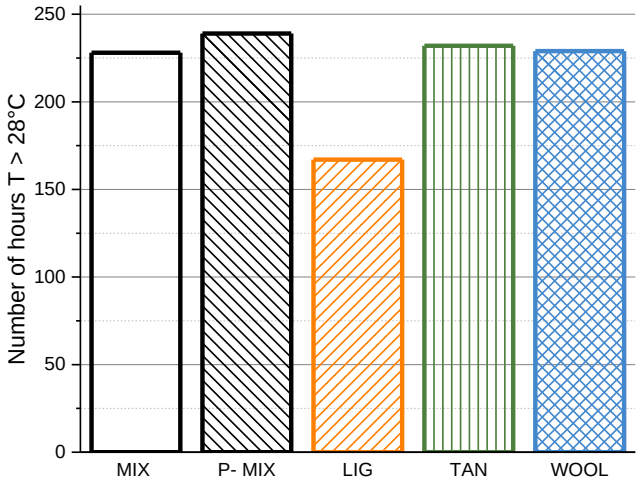


*Figure 11: Number of hours where the room temperature is over 28°C (annual values).*

Although the risk of overheating is mitigated by the ventilation system that controls the airflow rate from the outdoor environment, the building has around 230 h/year with a temperature over 28°C. The different materials for the vertical walls -- MIX, P-MIX, TAN, and WOOL -- yield similar values. The highest number of hours is shown by P-MIX, with an increase of about 5% compared to MIX. This result suggests that

limiting the moisture buffering of the RE walls may reduce thermal comfort during summer. On the other hand, no evidence of this behavior is given by the data of temperature at a daily scale (Figure 14). Conversely, LIG has the lowest number of hours that exceed 28°C: 167 h versus 228 h for MIX, a reduction of about 27%. The different behavior of LIG may be due to the different thermal conductivity, higher thermal diffusivity, and lower thermal resistance. An additional investigation was conducted to check the possible influence of the threshold effect. This was verified and excluded by repeating the calculation with two different threshold values (29°C and 27°C in addition to 28°C). In all cases, the difference between the number of hours with a temperature higher than the threshold for the different materials was maintained.

The boxplot in Figure 12 shows the indoor temperatures for the configurations with different wall materials during summer (June 22 to September 22). In all the configurations, the median and average temperatures in summer are around 26°C and the indoor temperature ranges between 23°C and 33°C. LIG has a slightly higher range of temperature variability, while the median temperature is marginally lower than for the other configurations. This behavior confirms the previous results on the number of hours with a temperature higher than 28°C, showing that LIG has slightly reduced thermal resistance. Consequently, the

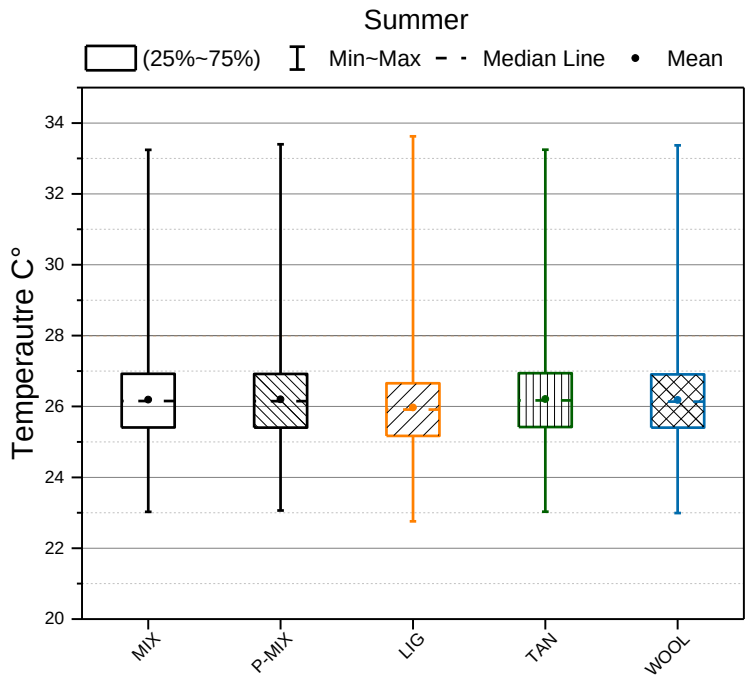


*Figure 12: Temperature box plot for different locations, scenarios, and wall materials during summer (June 22 to September 22). The maximal and minimal temperatures are reported, with the mean and median values of temperature.*

indoor temperature can follow the outdoor temperature faster, reaching higher values during the day but also cooling down the walls quickly during the night.

To better illustrate the physical behavior, Figure 13 presents the indoor and outdoor temperatures of the configurations with MIX walls. Only MIX is reported because the differences between the different materials are not appreciable at this scale. The outdoor temperature shows large daily variations, with an amplitude in the range of 10°C. In all the configurations, the indoor temperatures have a similar daily variation, within a range of 4°C. The inertia of RE maintains a stable temperature in the indoor environment during the day. The night ventilation increased from 22:00 to 08:00 (2 volume/h), from June to August, favoring cooling during the night (when the outdoor temperature is lower) to release the heat stored during the day. Considering the graph in Figure 13, some canicular events can be identified, where the temperature remains exceptionally high for 2–3 days consecutively. In this case, the inertia of the building is particularly useful for avoiding extremely high temperatures, maintaining a difference of 10°C between the indoor and outdoor environments during the highest peak of temperature in the day. A similar behavior was observed by Becket et al. [22] during summer canicular events in an RE house built in the hot-arid climate of Western Australia. Fernandes et al. [63] also presented the results of a measurement campaign in southern Portugal on a vernacular RE building. They found more variability in the temperature buffering, with recurrent values of around 8°C difference between outdoor and indoor conditions, and exceptionally a difference of 11°C. Soudani [13] observed a maximal buffering in temperature equal to 9°C for an RE house located in Isère, south-eastern France. The highest daily difference of 15°C was observed by Bassoud et al. [64] in mud bricks in adobe building in Adrar (southern Algeria), classified as arid desert areas. These examples illustrate the good performance of earthen houses, thereby guaranteeing thermal comfort in summer. This behavior may be particularly beneficial in a scenario of climate change, where canicular episodes are expected to be recurrent. Moreover, the ventilation schedule may be adapted and augmented to allow for faster cooling of the material on the days following the canicular episode. Figure 14 reports the daily variation of temperature of the outdoor and indoor environments, compared to the variation of the average water content in the south wall. The graph compares 3 days and only the results of MIX, P-MIX, and LIG are reported because at a daily scale the differences between other materials are not appreciable. Therefore, the results achieved

with MIX are considered representative of TAN, WOOL, and P-MIX results. The P-MIX temperatures almost overlap the results of MIX. LIG shows slightly lower temperatures in the indoor environment, in particular during the day, while the night temperatures are probably more uniform due to the higher ventilation rate. These differences are still minimal, but their impact is evident in Figure 11 and Figure 12 that present statistics at a seasonal scale, in particular for the number of hours at temperatures higher than 28°C. The oscillation of temperature in the external environment is ±5°C, while for both cases the indoor environment is maintained in a range of ±1.5° C.

Considering the wall moisture content, all the materials show similar values, between 0.385% and 0.398%. PMIX shows a slightly lower moisture content than MIX and LIG, with a daily cycle of moisture and adsorption release of slightly lower amplitude. Since the indoor environment is the main source of moisture, the presence of the painting reduces the adsorption of water vapor by the wall, both as storage and buffering. Observing the case of P-MIX, at daily scale the impact of using a layer of painting on the indoor temperature is not remarkable, while at the scale of 1 year some differences are evident (Figure 11). The daily fluctuation of moisture content in the walls is low, reaching its maximal value in the morning around 09:00–10:00; then, due to temperature rise, the evaporation of moisture occurs until 18:00–19:00, when the minimum value is reached.

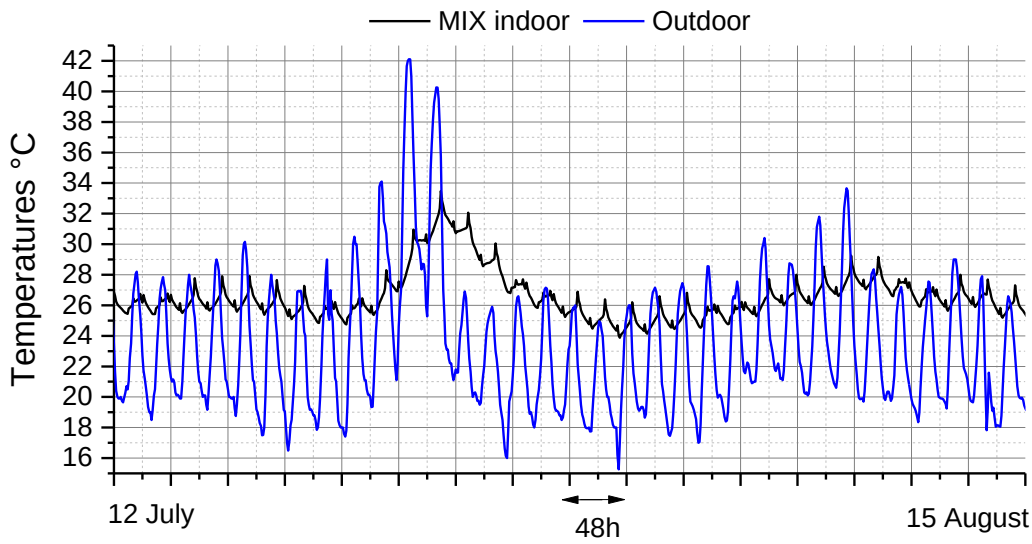


*Figure 13: Temperature variations of the indoor and outdoor air in the configuration with MIX walls.*

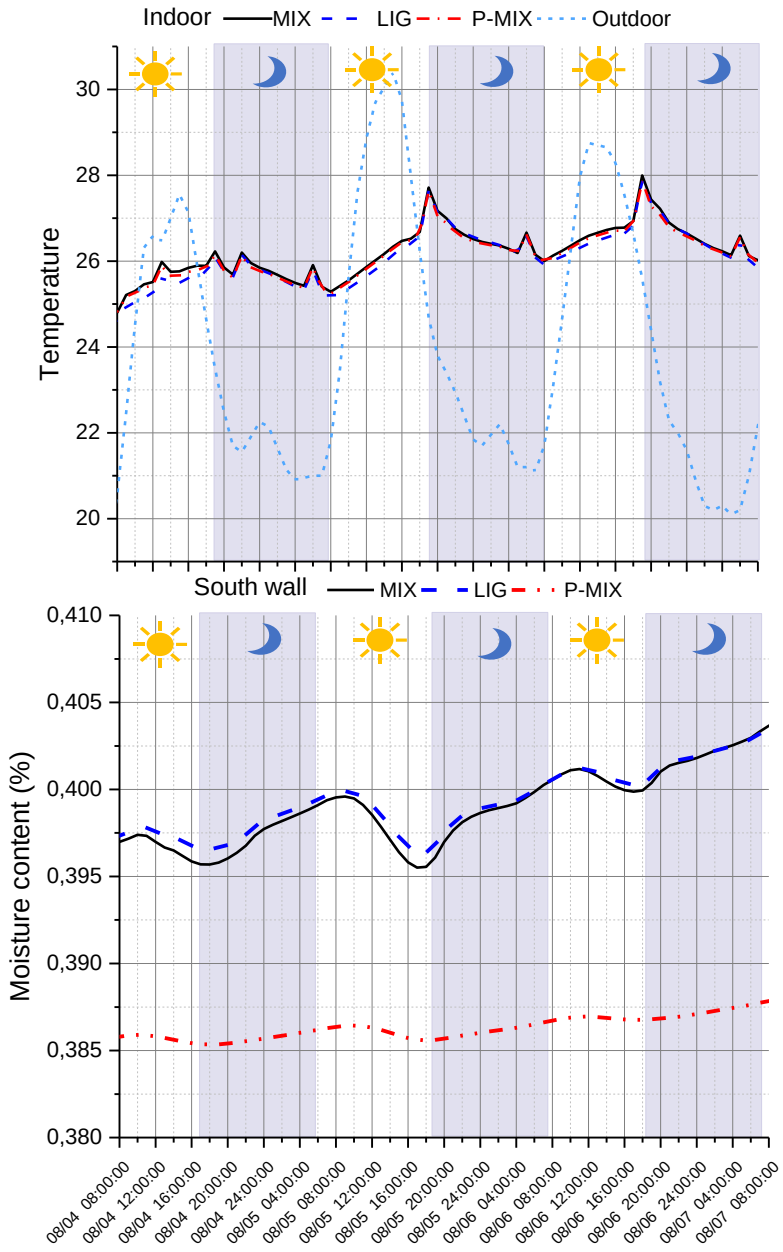


*Figure 14: Daily variation of temperature in indoor and outdoor enviromnment, with the indoor surface temperature variation, compared with the moisture variations in the south wall.*

Observing the daily temperature variation during summer, it is possible to identify a daily thermal lag that makes the indoor environment reach the maximal temperature when the outdoor temperature is already descending, with a delay of about 5 h. As shown in Figure 14, the maximal outdoor temperature is reached around 14:00–15:00, while the maximal indoor temperature is reached at 17:00. A similar thermal lag (6 h) for RE walls was previously measured by Soudani et al. [10,13], for an RE house with a wall thickness of 50 cm. Bassoud et al. [64] also measured a phase difference of 4 h between the indoor and outdoor temperature for an adobe house in Algeria, in the region of Adrar. For a broader case study consideration,

Beckett et al. [65] present a range of RE thermal lag values, which can vary from 1 to 10 h, depending on the density and thickness of the walls but also on the geometry of the dwelling and the occupancy scenarios.

### 4.2.3 Indoor air humidity and latent balance

The European standard EN15251 for indoor air quality simulation [62] indicates different ranges of RH comfort zones for different categories. Category II (from 25% to 60% RH) was chosen to evaluate the comfort range of RH in the results of the simulation. The standard considers a heating set point at 20°C and a cooling setpoint at a temperature of 26°C; the latter is absent in the present study and only substituted by a ventilation system [62]. Owing to the absence of a cooling system, the maximal temperature and humidity reached are higher in the present study.

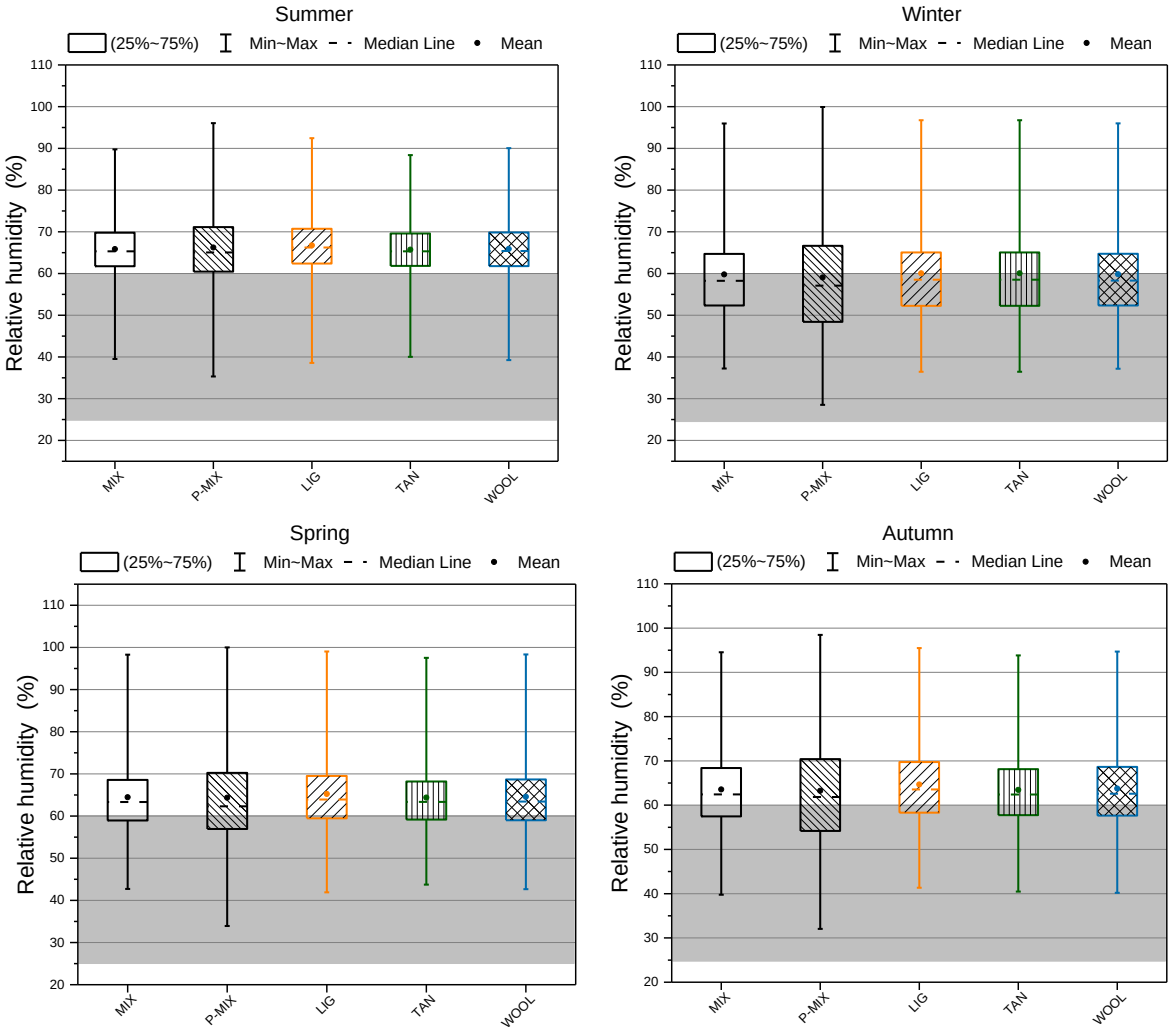


*Figure 15: Box-plot of the seasonal relative humidity values for the different configurations. Winter (December 22 to March 21), summer (June 22 to September 22), spring (21 March to June 22), and autumn (September 22 to December 22).*

Figure 15 presents the annual indoor humidity, during spring (March 22 to June 21), autumn (June 23 to September 21), winter (December 22 to March 21), and summer (June 22 to September 22), with a gray band to show the range of the comfort zone in accordance with the European standard EN15251. The different materials of the vertical walls – WOOL, LIG, and MIX – yield similar values. By contrast, P-MIX presents higher extreme values out of the comfort zone, as a consequence of the reduced buffering capacity. For TAN, the highest values for RH are slightly reduced in comparison with the other materials, in particular during summer and spring.

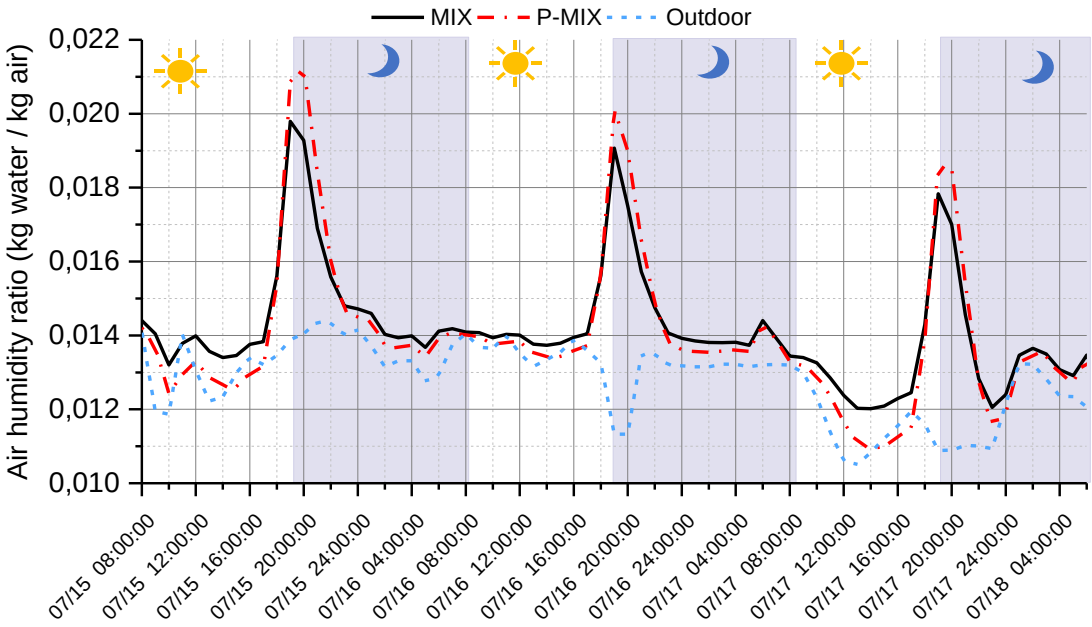


*Figure 16: Weekly variation of air humidity ratio in the outdoor climate of Casablanca and the indoor environment with MIX (representative of LIG, TAN, and WOOL configurations) and P-MIX*

To provide more detailed insight into the physical behavior, Figure 16 reports the daily variations of the outdoor and indoor humidity ratios for P-MIX and MIX configurations. The daily peaks of moisture are related to cooking activities during dinner. P-MIX shows the widest daily variation in humidity ratio, while MIX shows a slightly better ability to reduce these peaks in moisture. The impact of the other RE materials (not shown in the graphs for the sake of clarity) is very similar. WOOL and LIG present the same cycles as MIX, while TAN reduces minimally the variation of indoor humidity.

At a yearly scale, occupancy is the principal contribution to the latent gain, due to the anthropic presence and activities that produce moisture. It accounts for about 67% of the latent gain for MIX, TAN, LIG, and WOOL, while the desorption of RE walls represents 31% of the latent gain contribution. For the P-MIX configuration, by contrast, almost all of the latent gain is due to occupancy activities (98%). Similarly, the latent loss is principally attributed to ventilation (93%) while RE walls for MIX, TAN, LIG, and WOOL contribute about 6% to latent loss. Again, P-MIX walls have an almost negligible contribution to moisture buffering and they do not contribute to latent losses. These results show clearly that RE walls without paint adsorb and release water vapor, contributing to buffer moisture variations in the indoor environment.

# 5 Conclusions and outlook

Three biopolymers (lignin sulfonate, tannins, and wool) were tested as RE stabilizers. The modifications in the hygrothermal properties at the material scale were found to be significant only in the case of thermal conductivity of RE stabilized with lignin sulfonate, which was increased by about 30% compared with the control samples. The hygrothermal characterization was used to describe the material properties necessary as input data for a whole-building simulation using a combined heat and moisture transfer model in EnergyPlus. Various configurations were tested with vertical walls made of the different RE stabilized materials, considering a warm climate with a residential scenario for the occupancy.

The use of RE walls stabilized with lignin sulfonate results in an increment of the heating demand by about 32%, probably due to the higher thermal conductivity, while the thermal comfort is slightly improved. At a yearly scale, the uninsulated RE walls represent approximately 50% of the total sensible heat losses. All RE walls are effective in reducing temperature oscillations, particularly in the case of canicular events, where the indoor temperature can be reduced by up to 10° compared with the outdoor temperature. The ventilation during summer nights was particularly effective in evacuating the heat stored in the walls during the day.

The indoor humidity benefits from the passive regulation by RE walls, whereas applying paint on the indoor surface (painted MIX) reduces this effect significantly with a higher number of hours out of the comfort zone. On a yearly scale, RE walls (except painted MIX) represent 31% of the latent gain (desorption)

for indoor air, while the contribution of RE to the latent losses (adsorption) is only about 6%; indoor moisture is removed mainly by ventilation. The contribution of the walls to vapor exchange is remarkable when compared with the configuration with paint, which should be avoided in the case of RE walls.

Concluding, the strategy used to characterize the material properties and simulate their impact on the whole-building scale offers a new interesting possibility of analysis and investigation of RE materials, in particular using HAMT simulation to compare materials under realistic climate conditions and occupancy scenarios. The use of HAMT simulations combined with characterization at the material scale provides a more extensive investigation approach, which opens the possibility of research in different directions, promoting the study of the impact of hygrothermal properties and the use of RE materials for different climates and occupancy scenarios.

**Author Contributions:** Experimental Investigation, A.E.L. and L.V.; sorption isotherm, A.L.; water vapor permeability and thermal conductivity, A.L. and L.V.; Simulation, A.E.L. and L.V.; formal analysis, A.E.L., M.W. and A.-C.G.; resources, M.W. and A.-C.G.; data curation, A.E.L.; writing—original draft preparation, A.E.L.; writing—review and editing, A.E.L., M.W.; visualization, A.E.L., M.W.; supervision, M.W., G.D. and A.-C.G.; project administration, A.E.L., M.W., G.D. and A.-C.G.; funding acquisition, A.-C.G., G.D. and M.W.; conceptualization A.E.L. and M.W. , A.-C.G. All authors have read and agreed to the published version of the manuscript.

**Funding:** This research was funded by MOPGA (Make our Planet Great Again) grant number [926275K] and OLIMP (ADEME) grant number [1904C0019].

**Institutional Review Board Statement**: Not applicable. Informed Consent Statement: Not applicable.

**Data Availability Statement:** The data reported in this article are available in the thesis defended on 13 December 2021 by Alessia Emanuela Losini; the title of the dissertation is “Rammed earth stabilization with waste or recycled materials and natural additives: characterization and simulation.”

**Acknowledgments:** The authors would like to acknowledge Jonathan Outin for his contribution to the heat-specific analysis. The financial support for the Doctoral Program of research was given by Make Our

Plane Great Again and Universite Savoie Mont Blanc, France. The work also benefited from the OLIMP, Smart-Reno projects and TERAC financial support and has been supported by the French National Research Agency, through the Investments for Future Program (ref. ANR-18-EURE-0016 – Solar Academy). The authors would like to thank Minerali Industriali S.r.l., Dal Zotto S.r.l., Silvateam S.p.a, a. (San Michele Mondovì CN, Italy), Burgo Group (Mosaico S.r.l., Vicenza, Italy) and The Wool Biella Company for the materials supplied to run the experimentation.

# 6 Bibliography

[1] IEA, World Energy Outlook 2022,INTERNATIONAL ENERGY AGENCY, 2022. https://www.iea.org/Reports/World-Energy-Outlook-2022/Executive-Summary.

[2] Ministre de la Transition écologique, RE 2020 Éco-construire pour le confort de tous - dossier de presse, 2020. http://rt-re-batiment.developpement-durable.gouv.fr/IMG/pdf/dp_re2020.pdf (accessed October 19, 2022).

[3] G. Minke, Building with earth, Design and Technology of a Sustainable Architecture, Birkhäuser – Publishers for Architecture, 2012.

[4] R. Anger, L. Fontaine, Bâtir en terre: du grain de sable à l'architecture, Belin, Cit, Paris, France, 2009.

[5] M.R. Hall, R. Lindsay, M. Krayenhoff, Modern Earth Buildings: Materials, Engineering, Constructions and Applications, 2012. https://doi.org/10.1533/9780857096166.

[6] Q.-B.B. Jean-Claude Morel , Rabia Charef , Erwan Hamard , Antonin Fabbri , Chris Beckett, Earth as construction material in the circular economy context: practitioner perspectives on barriers to overcome, Philos. Trans. R. Socoiety. (2021).

[7] S.E. Hale, A.J. Roque, G. Okkenhaug, E. Sørmo, T. Lenoir, C. Carlsson, D. Kupryianchyk, P. Flyhammar, B. Žlender, The reuse of excavated soils from construction and demolition projects: Limitations and possibilities, Sustain. 13 (2021) 1–15. https://doi.org/10.3390/su13116083.

[8] F. Pacheco-Torgal, S. Jalali, Earth construction: Lessons from the past for future eco-efficient construction, Constr. Build. Mater. 29 (2012) 512–519.

https://doi.org/10.1016/j.conbuildmat.2011.10.054.

[9] G. Minke, Building with earth, Walter de Gruyter, 2012.

[10] H. Philippe, J. Morel, A. Fabbri, L. Soudani, C. Florient, N. Meunier, L ' ISOLATION DU PISÉ : PERTINENCE et principes, LGCB-ENTPE - TransLettre Août 2015. (2015) 1–12. https://doi.org/10.13140/RG.2.1.1238.1688.

[11] G. Giuffrida, M. Detommaso, F. Nocera, R. Caponetto, Design Optimisation Strategies for Solid Rammed Earth Walls in Mediterranean Climates, Energies 2021, Vol. 14, Page 325. 14 (2021) 325. https://doi.org/10.3390/EN14020325.

[12] B. Marques, H. Varum, H. Corvacho, M.C. Guedes, L. Baptista, Using Raw Earth Construction Systems on Contemporary Buildings: Reflections on Sustainability and Thermal Efficiency, Renew. Energy Environ. Sustain. 6 (2021) 46. https://doi.org/10.1051/rees/2021041.

[13] L. Soudani, Modelling and experimental validation of the hygrothermal performances of earth as a building material, Thesis at University of Lyon, 2016. Thesis in Civil Engineerin.

[14] D. Ciancio, P. Jaquin, P. Walker, Advances on the assessment of soil suitability for rammed earth, Constr. Build. Mater. 42 (2013) 40–47. https://doi.org/https://doi.org/10.1016/j.conbuildmat.2012.12.049.

[15] P. Chauhan, A. El Hajjar, N. Prime, O. Plé, Unsaturated behavior of rammed earth: Experimentation towards numerical modelling, Constr. Build. Mater. 227 (2019) 116646. https://doi.org/10.1016/j.conbuildmat.2019.08.027.

[16] B. V. Venkatarama Reddy, P. Prasanna Kumar, Embodied energy in cement stabilised rammed earth walls, Energy Build. 42 (2010) 380–385. https://doi.org/10.1016/j.enbuild.2009.10.005.

[17] A. Arrigoni, A.C. Grillet, R. Pelosato, G. Dotelli, C.T.S. Beckett, M. Woloszyn, D. Ciancio, Reduction of rammed earth's hygroscopic performance under stabilisation: an experimental investigation, Build. Environ. 115 (2017) 358–367. https://doi.org/10.1016/j.buildenv.2017.01.034.

[18] M. Saidi, A.S. Cherif, B. Zeghmati, E. Sediki, Stabilization effects on the thermal conductivity and sorption behavior of earth bricks, Constr. Build. Mater. 167 (2018) 566–577.

[19] A.E. Losini, A.-C. Grillet, M. Woloszyn, L. Lavrik, C. Moletti, G. Dotelli, M. Caruso, Mechanical and

Microstructural Characterization of Rammed Earth Stabilized with Five Biopolymers, Mater. . 15 (2022). https://doi.org/10.3390/ma15093136.

[20] A.E. Losini, A.C. Grillet, M. Bellotto, M. Woloszyn, G. Dotelli, Natural additives and biopolymers for raw earth construction stabilization – a review, Constr. Build. Mater. 304 (2021) 124507. https://doi.org/10.1016/j.conbuildmat.2021.124507.

[21] M. Hall, D. Allinson, Analysis of the hygrothermal functional properties of stabilised rammed earth materials, Build. Environ. 44 (2009) 1935–1942. https://doi.org/10.1016/j.buildenv.2009.01.007.

[22] C.T.S. Beckett, R. Cardell-Oliver, D. Ciancio, C. Huebner, Measured and simulated thermal behaviour in rammed earth houses in a hot-arid climate. Part B: Comfort, J. Build. Eng. (2017). https://doi.org/10.1016/j.jobe.2017.07.013.

[23] L. Daniel, V. Soebarto, T. Williamson, House energy rating schemes and low energy dwellings: The impact of occupant behaviours in Australia, Energy Build. 88 (2015) 34–44. https://doi.org/10.1016/j.enbuild.2014.11.060.

[24] G. Giuffrida, R. Caponetto, F. Nocera, M. Cuomo, Prototyping of a Novel Rammed Earth Technology, Sustain. 2021, Vol. 13, Page 11948. 13 (2021) 11948. https://doi.org/10.3390/SU132111948.

[25] P. Taylor, R.J. Fuller, M.B. Luther, Energy use and thermal comfort in a rammed earth office building, Energy Build. 40 (2008) 793–800. https://doi.org/10.1016/j.enbuild.2007.05.013.

[26] D. Medjelekh, L. Ulmet, F. Dubois, Characterization of hygrothermal transfers in the unfired earth, Energy Procedia. 139 (2017) 487–492. https://doi.org/10.1016/j.egypro.2017.11.242.

[27] J. Tan, J. Liang, L. Wan, B. Jiang, Influence of Non-Constant Hygrothermal Parameters on Heat and Moisture Transfer in Rammed Earth Walls, Buildings. 12 (2022). https://doi.org/10.3390/buildings12081077.

[28] B. Jiang, T. Wu, W. Xia, J. Liang, Hygrothermal performance of rammed earth wall in Tibetan Autonomous Prefecture in Sichuan Province of China, Build. Environ. 181 (2020) 107128. https://doi.org/10.1016/j.buildenv.2020.107128.

[29] D. Allinson, M. Hall, Hygrothermal analysis of a stabilised rammed earth test building in the UK, Energy Build. 42 (2010) 845–852. https://doi.org/10.1016/j.enbuild.2009.12.005.

[30] M. Krus, K. Kießl, Determination of the moisture storage characteristics of porous capillary active materials M. Krus, K. Kießl Fraunhofer-Institut für Bauphysik, Holzkirchen, Germany, (1995) 1–17.

[31] J. Goffart, M. Rabouille, N. Mendes, Uncertainty and sensitivity analysis applied to hygrothermal simulation of a brick building in a hot and humid climate, J. Build. Perform. Simul. 10 (2017) 37–57. https://doi.org/10.1080/19401493.2015.1112430.

[32] U.S. Department of Energy, Engineering Reference, EnergyPlus™ Version 9.4.0 Documentation, (2020).

[33] A.E. Losini, L. Lavrik, M. Caruso, M. Woloszyn, A.C. Grillet, G. Dotelli, P. Gallo Stampino, Mechanical Properties of Rammed Earth Stabilized with Local Waste and Recycled Materials, in: Bio-Based Build. Mater., Trans Tech Publications Ltd, 2022: pp. 113–123. https://doi.org/10.4028/www.scientific.net/cta.1.113.

[34] Annual Book of ASTM Standards, ASTM D1557-07 Standard Test Methods for Laboratory Compaction Characteristics of Soil Using Modified Effort, West Conshohocken, United States, 2007. https://doi.org/10.1520/D1557-07.1.

[35] ISO 12571:2013(E), International Standard Hygrothermal performance of building materials and products — Determination of hygroscopic sorption properties, 2013.

[36] L. Greenspan, Humidity fixed points of binary saturated aqueous solutions, J. Res. Natl. Bur. Stand. - A. Phys Ics Chem. 81 (1977).

[37] Direction Collectif Terre Crue, Buge - Guide des bonnes pratiques de la constuction en terre crue, edition 13 decembre, France, 2018.

[38] C. Rode, Moisture Buffering of Building Materials Department of Civil Engineering Technical University of Denmark, 2005.

[39] NSAI, EN ISO 12572 - Hygrothermal performance of building materials and products - Determination of water vapour transmission properties, (2001) 1–35.

[40] D.M. Nguyen, A.C. Grillet, T.M.H. Diep, Q.B. Bui, M. Woloszyn, Characterization of hygrothermal insulating biomaterials modified by inorganic adsorbents, Heat Mass Transf. Und Stoffuebertragung. 56 (2020) 2473–2485. https://doi.org/10.1007/s00231-020-02873-2.

[41] R.L. Danley, New heat flux DSC measurement technique, Thermochim. Acta. 395 (2002) 201–208. https://doi.org/10.1016/S0040-6031(02)00212-5.

[42] M. Thommes, K. Kaneko, A. V. Neimark, J.P. Olivier, F. Rodriguez-Reinoso, J. Rouquerol, K.S.W. Sing, Physisorption of gases, with special reference to the evaluation of surface area and pore size distribution (IUPAC Technical Report), Pure Appl. Chem. 87 (2015) 1051–1069. https://doi.org/10.1515/pac-2014-1117.

[43] L. Soudani, M. Woloszyn, A. Fabbri, J.C. Morel, A.C. Grillet, Energy evaluation of rammed earth walls using long term in-situ measurements, Sol. Energy. 141 (2017) 70–80. https://doi.org/10.1016/j.solener.2016.11.002.

[44] F. McGregor, A. Heath, A. Shea, M. Lawrence, The moisture buffering capacity of unfired clay masonry, Build. Environ. 82 (2014) 599–607. https://doi.org/10.1016/j.buildenv.2014.09.027.

[45] A. Fabbri, F. McGregor, I. Costa, P. Faria, Effect of temperature on the sorption curves of earthen materials, Mater. Struct. 50 (2017) 253.

[46] M. Labat, C. Magniont, N. Oudhof, J.-E. Aubert, From the experimental characterization of the hygrothermal properties of straw-clay mixtures to the numerical assessment of their buffering potential, Build. Environ. 97 (2016) 69–81. https://doi.org/https://doi.org/10.1016/j.buildenv.2015.12.004.

[47] P. Chabriac, Mesure du comportement hygrothermique du pisé Pierre-Antoine, Thesis at University of Lyon, 2014. https://hal.archives-ouvertes.fr/tel-01413611.

[48] N.D. Mao, Panels from bamboo fibers/powders for building construction: elaboration and hygrothermal characterization, Thesis at Université Savoie Mont Blanc, Le burget du lac, 2016.

[49] Redige sous Direction Collectif des Associaiton et Federation Terre Crue, Guide des bonnes pratiques de la constuction en terre crue, complet, edition 13 décembre 2018, n.d. https://www.rehabilitation-bati-ancien.fr/espace-documentaire/guide-des-bonnes-pratiques-la-construction-en-terre-crue [18/04/2022].

[50] M. Hall, D. Allinson, Assessing the effects of soil grading on the moisture content-dependent thermal conductivity of stabilised rammed earth materials, Appl. Therm. Eng. 29 (2009) 740–747.

https://doi.org/10.1016/j.applthermaleng.2008.03.051.

[51] G. Giuffrida, R. Caponetto, F. Nocera, Hygrothermal properties of raw earth materials: A literature review, Sustain. 11 (2019). https://doi.org/10.3390/su11195342.

[52] L. Randazzo, G. Montana, A. Hein, A. Castiglia, G. Rodonò, D.I. Donato, Moisture absorption, thermal conductivity and noise mitigation of clay based plasters: The influence of mineralogical and textural characteristics, Appl. Clay Sci. 132–133 (2016) 498–507. https://doi.org/10.1016/j.clay.2016.07.021.

[53] J. Neymark, R. Judkoff, International Energy Agency Building Energy Simulation Test and Diagnostic Method for Heating, Ventilating, and Air-Conditioning Equipment Models (HVAC BESTEST), (2002) 350. http://www.nrel.gov/docs/fy02osti/30152.pdf.

[54] V. Maniatidis, P. Walker, A review of rammed earth construction, 2003. http://staff.bath.ac.uk/abspw/rammedearth/review.pdf.

[55] P.A. Jaquin, C.E. Augarde, C.M. Gerrard, Chronological description of the spatial development of rammed Earth techniques, Int. J. Archit. Herit. 2 (2008) 377–400. https://doi.org/10.1080/15583050801958826.

[56] D. Verner, D. Treguer, J. Redwood, J. Christensen, R. McDonnell, C. Elbert, Y. Konishi, S. Belghazi, Climate Variability, Drought, and Drought Management in Morocco's Agricultural Sector, 2018. https://doi.org/10.1596/30603.

[57] R. El-Nabouch, Q.B. Bui, O. Plé, P. Perrotin, Characterizing the shear parameters of rammed earth material by using a full-scale direct shear box, Constr. Build. Mater. 171 (2018) 414–420. https://doi.org/10.1016/j.conbuildmat.2018.03.142.

[58] M. Labat, M. Woloszyn, Moisture balance assessment at room scale for four cases based on numerical simulations of heat–air–moisture transfers for a realistic occupancy scenario, J. Build. Perform. Simul. 9 (2016) 487–509. https://doi.org/10.1080/19401493.2015.1107136.

[59] B. Poirier, G. Guyot, H. Geoffroy, M. Woloszyn, M. Ondarts, E. Gonze, Pollutants emission scenarios for residential ventilation performance assessment. A review, J. Build. Eng. 42 (2021). https://doi.org/10.1016/j.jobe.2021.102488.

[60] ASHRAE (American Society of Heating Refrigerating and Air-conditioning Engineers), Handbook HVAC

fundamentals, 2009.

[61] A. Stefanoiu, A.M. Stefanoiu, Towards performance evaluation of energy efficient buildings To cite this version : HAL Id : tel-01706622 Vers l ' évaluation de la performance des bâtiments à haute efficacité énergétique, 2017.

[62] E. Standard, UNI Standard EN15251. Indoor environmental input parameters for design and assessment of energy performance of buildings addressing indoor air quality, thermal environment, lighting and acoustics. European committee for Standardization, (2007).

[63] J. Fernandes, R. Mateus, H. Gervásio, S.M. Silva, L. Bragança, Passive strategies used in Southern Portugal vernacular rammed earth buildings and their influence in thermal performance, Renew. Energy. 142 (2019) 345–363. https://doi.org/10.1016/j.renene.2019.04.098.

[64] A. Bassoud, H. Khelafi, A.M. Mokhtari, A. Bada, Evaluation of summer thermal comfort in arid desert areas. Case study: Old adobe building in Adrar (South of Algeria), Build. Environ. 205 (2021) 108140. https://doi.org/10.1016/j.buildenv.2021.108140.

[65] C.T.S. Beckett, R. Cardell-Oliver, D. Ciancio, C. Huebner, Measured and simulated thermal behaviour in rammed earth houses in a hot-arid climate. Part A: Structural behaviour, J. Build. Eng. 15 (2018) 243–251. https://doi.org/10.1016/j.jobe.2017.11.013.